Theor Chem Acc (2012) 131:1106
DOI 10.1007/s00214-012-1106-1

REGULAR ARTICLE

Chemical bonding descriptors based on electron density inhomogeneity measure: a comparison with ELI-D

K. Finzel · Yu. Grin · M. Kohout

Received: 5 July 2011 / Accepted: 18 July 2011 / Published online: 9 February 2012

Abstract The electron localizability indicator (ELI-D) is suitable to describe certain aspects of the bonding situation of molecules and solids. ELI-D is based on integrals of electron pair density over very small regions. Recently proposed functional C_p, derived from the electron population in regions of fixed amount of electron density inhomogeneity, is based on the same approach as ELI-D, that is, ω-restricted space partitioning. The electron density inhomogeneity is given by the distance of electron density values to the averaged density within chosen region. Thus, in contrast to ELI-D, C_p is a single-electron property. The distance measure depends on a parameter that can be optimized in such way that C_p mimics the topology of the ELI-D distribution for atoms. Such an optimization was performed for the atoms Li to Xe. The optimal parameter $p = 0.6$ yields the functional $C_{0.6}$ that was exemplary applied to a few chosen molecules. In case of molecules the topology of the inner shell and lone-pair regions as given by $C_{0.6}$ is comparable with that of the ELI-D representation. However, in the bonding region between the atoms the topology of $C_{0.6}$ is dominated by the low density gradient close to the bond critical point. This may result in rather different topologies when comparing $C_{0.6}$ and ELI-D.

Keywords Bonding · Electron density · Inhomogeneity measure · Space partitioning · Molecules

K. Finzel (✉) · Yu. Grin · M. Kohout
Max-Planck-Institut für Chemische Physik fester Stoffe, Nöthnitzer Str. 40, 01187 Dresden, Germany
e-mail: kati.finzel@cpfs.mpg.de

1 Introduction

The onerous vision of chemistry is to understand molecular and solid state systems in terms of descriptors referring to relation between their atomic components. Therefore, the chemical bond remains in the foreground of ongoing theoretical research. Unfortunately, there is no quantum mechanically defined operator for the chemical bond. This gives rise to rather ambiguous interpretations of bonding situations. Despite this rather pessimistic statement (or possibly just because of it) it is necessary to utilize several different approaches, each of which accentuating specific viewpoint, to shed more light on this problem.

There are various methods used to examine the bonding situation even when focusing on the real space analyses only. For instance, the quantum theory of atoms in molecules (QTAIM) of Bader is widely applied concept [1]. The most important quantity in QTAIM is the electron density serving as the basis on which the atomic basins are defined, the critical points and bond paths (forming a molecular graph) are determined, as well as other related properties, like the density Laplacian, virial ratio or the populations of atomic basins, are evaluated. The QTAIM basins are often used for partitioning schemes, for example, for the energy decomposition [2, 3]. Another function derived from the electron density is the logarithmic density gradient [4] which can also be utilized for the bonding analysis [5]. The ratio between the density Laplacian and the distance to a reference position defines the local source [6]. The integral of local source over chosen region (e.g., QTAIM basins) yields the source function, describing how the region participate on the reconstruction of the electron density at the reference position [7]. From the electron density, its gradient and Laplacian the one-electron potential (OEP) can

be computed [8]. The negative of OEP is connected with the kinetic energy of an electron. Regions of negative OEP (where electrons are classically allowed) can be attributed to atomic shells [9, 10], lone-pairs and bonds between atoms [8], respectively.

Yet another bundle of methods for bonding analysis is based on the electron pair density. The evaluation of specific part of pair density integrals over basins leads to the localization and delocalization indexes [11]. Approaches utilizing the pair density are often connected with the notion of 'electron localization', for example, the electron localization function (ELF) [12], which is a ratio between two functions—the curvature of Fermi hole at the examined position and that of a uniform electron gas (arbitrary chosen reference system) with the same electron density. Related to ELF is the spin-pair composition [13]. Here, the number of same-spin pairs is compared to the number of opposite-spin pairs in small but otherwise arbitrary region. Likewise, with the integrals of pair density (and electron density as well) is defined the electron localizability indicator ELI [14]. ELI follows different philosophy than the spin-pair composition. The values of its variant ELI-D [15–17] are proportional to the electron populations (charges) in regions enclosing fixed amount of electron pairs. The space partitioning into such regions (micro-cells) is given at once for the whole system and is controlled by so-called ω-restricted space partitioning (ωRSP) [18]. In contrast to the spin-pair composition, which is a continuous function, ELI is a quasi-continuous distribution of values [18].

Recently, the charge sampling functional C_p was proposed [19], which is proportional to charges in micro-cells enclosing fixed amount of electron density inhomogeneity (note the similarity with ELI-D where the charge is sampled over region of fixed electron pair fraction). The inhomogeneity measure is given by the distance of function values to the average value within chosen region (in case of C_p the electron density in a micro-cell). Thus, only single-electron functions are involved in the determination of C_p. As the distance measure depends on the parameter p (cf. next section) that can be freely chosen, this approach offers the opportunity to approximate ELI-D with the charge sampling functional by choosing proper distance measure. In the following the optimal inhomogeneity measure parameter p is determined for which the C_p distribution resembles the topology of the ELI-D distribution for atoms as close as possible. This procedure tries to approximate the so-called pair-volume function (connected with ELI-D) by single-electron functions. In a certain sense this means that the electron density inhomogeneity measure (functional of the electron density) was assumed to be related to the Fermi-hole curvature at the electron coalescence.

2 Theory

The concept of ω-restricted space partitioning (ωRSP) is a possible access to local interpretation of quantum mechanics [18, 20]. According to this approach, the space is subdivided into compact non-overlapping mutually exclusive space filling regions (micro-cells), each containing the same fixed amount of so-called control property. The idea behind this partitioning scheme is to 'probe' samples of the same 'quality' . After establishing such partitioning a second quantity is sampled within the micro-cells. The result is a discrete distribution of the sampled property values. Of course, the sampled values will scale with the chosen restriction value (which determines the actual size of the micro-cells). To remove this dependency, the sampled values are rescaled. The distribution of rescaled values is discrete by definition. However, because the restriction value is not specified, the distribution can be made as dense as one wishes (considering infinitesimally small restriction value). Distribution with such behavior is termed a quasi-continuous distribution [18] (with the limit after rescaling being a continuous function). Depending on the control and sampling functions, ωRSP gives rise to a family of quasi-continuous distributions.

If a single-electron function f_s is sampled, the resulting distribution $\{F_i\}$ can always be approximated by the following:

$$F_i \approx f_s \times V_\omega(\mu_i) \tag{1}$$

where $V_\omega(\mu_i)$ is the ω-restricted volume of the micro-cell μ_i. The ωRSP procedure assures all micro-cells to enclose the same amount of the control property ω. Distributions having either the sampling or the control function in common can easily be compared. In the following we compare the charge sampling functionals C_p and ELI-D. Both functionals are based on the sampling of electron density over micro-cells. The functionals differ in the function controlling the volume of the micro-cells, which are the pair density in case of ELI-D and the electron density inhomogeneity in case of C_p, respectively. In contrast to pair density, the electron density inhomogeneity measure is a single-electron function.

The distance $d_p(f, g)$ between the position $\mathbf{r}$ dependent functions $f(\mathbf{r})$ and $g(\mathbf{r})$ in a micro-cell μ_i having the volume $V(i)$ can be given by the integral:

$$d_p(f,g) = \sqrt[p]{\int_{\mu_i} |f(\mathbf{r}) - g(\mathbf{r})|^p \, dV} \tag{2}$$

with positive exponent p. This measure of distance is defined in the space $L_p(\mu_i)$ of functions f and g integrable with p-th power. If g is the average of the function $f(\mathbf{r})$ in the region μ_i, then the resulting distance can be interpreted

as an inhomogeneity measure of the function $f(\mathbf{r})$. In our case we are interested in the inhomogeneity $I_p(i)$ of the electron density $\rho(\mathbf{r})$ in the i-th micro-cell:

$$I_p(i) = \sqrt[p]{\int_{\mu_i} |\rho(\mathbf{r}) - \bar{\rho}_i|^p \, dV} \tag{3}$$

where the averaged density $\bar{\rho}_i$ in the region μ_i with the volume $V(i)$ is given by:

$$\bar{\rho}_i = \frac{1}{V(i)} \int_{\mu_i} \rho(\mathbf{r}) dV. \tag{4}$$

Expanding Eq. 3 in a Taylor series around the position $\mathbf{a}_i$ (for instance the center of the micro-cell μ_i) and successive integration yields for sufficiently small volumes:

$$I_p(i) \approx \frac{1}{2(p+1)^{1/p}} |\nabla\rho(\mathbf{a}_i)| \; V(i)^{(p+3)/3p}. \tag{5}$$

For an inhomogeneity I_p fixed at the value ω_{I_p} the above equation can be rearranged yielding the approximation of the corresponding micro-cell volume:

$$V_{I_p}(i) \;\approx\; \omega_{I_p}^{3p/(p+3)} \left[\frac{2(p+1)^{1/p}}{|\nabla\rho(\mathbf{a}_i)|}\right]^{3p/(p+3)}. \tag{6}$$

In sufficiently small micro-cell μ_i centered around the position $\mathbf{a}_i$ the charge is directly proportional to the volume:

$$q_i = \int_{\mu_i} \rho(\mathbf{r}) dV \approx \rho(\mathbf{a}_i) \; V_{I_p}(i). \tag{7}$$

Thus, the charge in a micro-cell with volume restricted by fixed electron density inhomogeneity is given by the expression:

$$q_i \;\approx\; \omega_{I_p}^{3p/(p+3)} \; \rho(\mathbf{a}_i) \left[\frac{2(p+1)^{1/p}}{|\nabla\rho(\mathbf{a}_i)|}\right]^{3p/(p+3)}. \tag{8}$$

We define the charge sampling functional C_p in the $L_p(\mu_i)$ space of the ωRSP micro-cells controlled by fixed infinitesimally small inhomogeneity value as the quasi-continuous distribution of rescaled charges (whereas $C_p(\mathbf{a}_i)\omega_{I_p}^{3p/(p+3)}$ is a discrete set of charges):

$$C_p(\mathbf{a}_i) = \frac{q_i}{\omega_{I_p}^{3p/(p+3)}} \approx \rho(\mathbf{a}_i) \left[\frac{2(p+1)^{1/p}}{|\nabla\rho(\mathbf{a}_i)|}\right]^{3p/(p+3)}. \tag{9}$$

The limit after rescaling (which is a continuous function):

$$\tilde{C}_p(\mathbf{r}) = \lim_{\omega\to 0}\{C_p(\mathbf{a}_i)\} = \rho(\mathbf{r}) \; \tilde{V}_{I_p}(\mathbf{r}) \tag{10}$$

includes the corresponding inhomogeneity-restricted volume function $\tilde{V}_{I_p}$ given by:

$$\tilde{V}_{I_p}(\mathbf{r}) = \left[\frac{2(p+1)^{1/p}}{|\nabla\rho(\mathbf{r})|}\right]^{3p/(p+3)}. \tag{11}$$

C_p is based on charges in micro-cells of fixed electron density inhomogeneity value. The volumes of the corresponding micro-cells are derived exclusively from a single-particle function, namely the electron density gradient. This can be compared to ELI-D (symbol Υ_D) which is based on charges in micro-cells enclosing fixed fraction ω_D of an electron pair [17]:

$$\Upsilon_D(\mathbf{a}_i) = \frac{q_i}{\omega_D^{3/8}} \approx \frac{1}{\omega_D^{3/8}} \; \rho(\mathbf{a}_i) \; V_D(i) \tag{12}$$

with the volume $V_D(i)$ of the ω_D-restricted micro-cell μ_i. For sufficiently small micro-cells the volume $V_D(i)$ can be approximated by the Fermi-hole curvature at the coalescence $g(\mathbf{a}_i)$ (derived from the pair density) [17]:

$$V_D(i) \;\approx\; \omega_D^{3/8} \left[\frac{12}{g(\mathbf{a}_i)|}\right]^{3/8}. \tag{13}$$

For ELI-D the limit after rescaling (continuous function) is given by:

$$\tilde{\Upsilon}_D(\mathbf{r}) = \rho(\mathbf{r}) \left[\frac{12}{g(\mathbf{r})}\right]^{3/8} = \rho(\mathbf{r}) \; \tilde{V}_D(\mathbf{r}) \tag{14}$$

where $\tilde{V}_D$ is the so–called pair-volume function. If the volumes of the micro-cell μ_i should be identical in both space partitioning procedures, i.e., $V_{I_p}(i) = V_D(i)$, the following condition had to be satisfied, cf. Eqs. 6 and 13:

$$\omega_{I_p}^{3p/(p+3)} \left[\frac{2(p+1)^{1/p}}{|\nabla\rho(\mathbf{a}_i)|}\right]^{3p/(p+3)} = \omega_D^{3/8} \left[\frac{12}{g(\mathbf{a}_i)|}\right]^{3/8}. \tag{15}$$

For an infinitesimally small micro-cell μ_i the ratio of restrictions producing identical micro-cell volumes approaches the value:

$$\left[\frac{\omega_{I_p}^{8p/(p+3)}}{\omega_D}\right]^{3/8} = \tilde{V}_D(\mathbf{a}_i) \;/\; \tilde{V}_{I_p}(\mathbf{a}_i). \tag{16}$$

The problem is to find such inhomogeneity measure parameter p for which for all $\mathbf{r}$ the ratio $\tilde{V}_D(\mathbf{r})/\tilde{V}_{I_p}(\mathbf{r})$ is as close as possible to a constant. The optimized p varies with the atomic species in the range of roughly 0.3–1.0 when p is evaluated in the atomic core regions.

For the application of C_p to molecules a single value (independent of atomic species) for the parameter p would be desirable. Thus, instead of the equivalence of the micro-cell volumes, the focus was set to sufficient reproduction of the ELI-D topology. As a suitable prescription seems to be

the equivalence of the logarithmic derivatives of the volume functions, i.e., $\nabla \ln \tilde{V}_{I_p}(\mathbf{r}) = \nabla \ln \tilde{V}_D(\mathbf{r})$, which leads to the condition:

$$\frac{\nabla \tilde{V}_{I_p}(\mathbf{r})}{\tilde{V}_{I_p}(\mathbf{r})} = \frac{\nabla \tilde{V}_D(\mathbf{r})}{\tilde{V}_D(\mathbf{r})}. \tag{17}$$

The relation to the ELI-D topology is given through:

$$\frac{\nabla \tilde{\Upsilon}_D(\mathbf{r})}{\tilde{\Upsilon}_D(\mathbf{r})} = \frac{\nabla \rho(\mathbf{r})}{\rho(\mathbf{r})} + \frac{\nabla \tilde{V}_D(\mathbf{r})}{\tilde{V}_D(\mathbf{r})} \tag{18}$$

and

$$\frac{\nabla \tilde{C}_p(\mathbf{r})}{\tilde{C}_p(\mathbf{r})} = \frac{\nabla \rho(\mathbf{r})}{\rho(\mathbf{r})} + \frac{\nabla \tilde{V}_{I_p}(\mathbf{r})}{\tilde{V}_{I_p}(\mathbf{r})}. \tag{19}$$

3 Results and discussion

The optimal inhomogeneity measure p, evaluated by least square fit to Eq. 17, was determined for atoms Li to Xe using the wave functions of Clementi and Roetti [21]. The volume functions have been calculated with the program DGrid [22]. The least square fit was performed within the distances from the nucleus ranging from 10^{-4} bohr up to the distance confining all but 0.1 electrons of the corresponding atom. The formalism of the theory part can be applied to the total density as well as to the majority and minority densities, respectively. The least square fit searching for the optimal inhomogeneity measure was done separately for each spin channel. The majority and minority volume functions ($\tilde{V}^{\alpha}_{I_p}$ and $\tilde{V}^{\beta}_{I_p}$, i.e., using the gradient of the corresponding σ-spin density) were adjusted to the corresponding same-spin pair-volume function ($\tilde{V}^{\alpha\alpha}_D$ and $\tilde{V}^{\beta\beta}_D$), whereas the total volume function ($\tilde{V}_{I_p}$) was adjusted to the triplet pair-volume function ($\tilde{V}^{(t)}_D$) [17].

The results of the least square fit procedures are shown in Fig. 1. As desired, the parameter p for the optimal inhomogeneity measure is nearly independent of the atomic number. Except for the fit of the minority component referring to the atoms B, C and N, all optimal inhomogeneity measures are concentrated around the value $p = 0.6$. Nevertheless, even for those atoms $p = 0.6$ is an acceptable choice for the minority channel. For the fit using the total electron density gradient the smallest value $p = 0.49$ is found for the B atom, the highest with 0.63 for the Mg atom. For further proceedings the inhomogeneity parameter was fixed at $p = 0.6$, in which case Eq. 9 reduces to:

$$C_{0.6}(\mathbf{a}_i) \approx \frac{8}{5^{5/6}} \frac{\rho(\mathbf{a}_i)}{\sqrt{|\nabla \rho(\mathbf{a}_i)|}}. \tag{20}$$

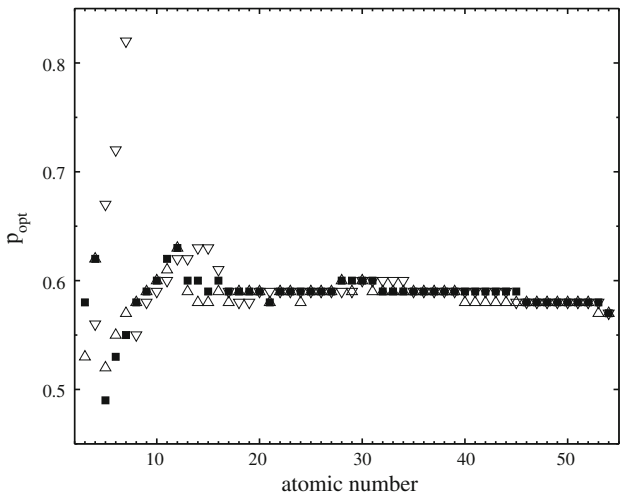

Fig. 1 Optimal inhomogeneity measure parameter p for the atoms Li to Xe. *Squares* fit using the total density gradient, *up triangles* fit for the majority spin component, *down triangles* fit for the minority spin component

The limit after rescaling can be expressed as:

$$\tilde{C}_{0.6}(\mathbf{r}) = \frac{8}{5^{5/6}} \sqrt{\rho(\mathbf{r})} \left[\frac{|\nabla \rho(\mathbf{r})|}{\rho(\mathbf{r})}\right]^{-1/2}. \tag{21}$$

Thus, the continuous function $\tilde{C}_{0.6}$ can be interpreted as a weighted average orbital. The weighting function can be linked with the local ionization potential $-|\nabla\rho| \,/\, \rho$ [4]. This interpretation applies only to the limit after rescaling. In contrast, the quasi-continuous distribution, cf. Eq. 20, is proportional to charges in micro-cells of the underlying space partitioning. The values are approximated by a product of the electron density and the volume function.

Note that $\tilde{C}_{0.6}$ bears similarity to the inverse of the reduced density gradient $s = |\nabla\rho|/(2k_F\ \rho) \propto |\nabla\rho|/\rho^{4/3}$ which plays an important role for the generalized gradient approximation [23–25] (in fact C_1 is proportional to $s^{-3/4}$ [19]). Recently the local behavior of the reduced density gradient was used to identify energetically important regions in solids [26].

Figure 2 shows the functionals $C_{0.6}$ (from total density) and triplet ELI-D, respectively, for the atoms Ne and Xe on logarithmic scale. In contrast to the standard triplet ELI-D, where the density of triplet-coupled electrons is sampled, the total electron density was sampled for better comparison with $C_{0.6}$. The distributions in Fig. 2 exhibit for both atoms similar structuring. While the atomic shell radii given by the minima of $C_{0.6}$ and ELI-D, respectively, are very similar, the maxima of $C_{0.6}$ are closer to the nucleus than the maxima of ELI-D. In case of the Ne atom even the values of $C_{0.6}$ are relatively close to the ones of ELI-D. This is no more valid for the heavier Xe atom, where the $C_{0.6}$ values are much higher than the ELI-D values,

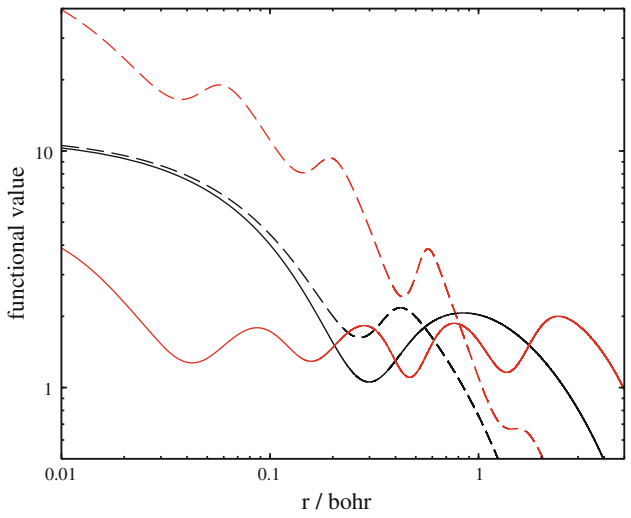

Fig. 2 Charge sampling functionals for the atoms Ne and Xe. *Black solid line* ELI-D for the Ne atom, *black dashed line* $C_{0.6}$ for the Ne atom, *red solid line* ELI-D for the Xe atom, *red dashed line* $C_{0.6}$ for the Xe atom. All data were computed from total density matrix

especially in the inner shell regions. Note that the inhomogeneity measure parameter p was chosen for $C_{0.6}$ to reproduce as closely as possible the ELI-D topology (the shell structuring), not the values itself. The charge sampling functional $C_{0.6}$ is easily transferable to molecular systems since the optimal inhomogeneity measure is independent of the atomic species.

The triplet ELI-D (sampling the total electron density) and the functional $C_{0.6}$ were compared for a few closed shell molecules. The wave functions have been calculated at the HF/cc-pVQZ level using Gaussian09 [27]. The calculation of the functionals as well as the evaluation of the basins was performed with DGrid [22]. A few remarks about $C_{0.6}$ can already be given without doing explicit calculations. $C_{0.6}$ is expected to show similar shell structuring as ELI-D in the region close to the atomic nuclei as it is not expected that the inner shell regions change significantly in molecular systems. However, in the valence region the topology of $C_{0.6}$ may deviate from that of ELI-D as $C_{0.6}$ is dominated by the low density gradient close to the bond critical point. There will be an attractor in $C_{0.6}$ at every bond critical point in the molecule, cf. Eq 20. Thus, from this simplistic viewpoint it can be expected that $C_{0.6}$ will display certain chemical signatures of a bound molecular system.

The diagrams in the left column of Fig. 3 show the functionals ELI-D and $C_{0.6}$ for the water molecule. The upper left diagram in Fig. 3 displays the 2.33-localization domains of ELI-D and the middle left diagram the 1.62-localization domains of $C_{0.6}$. The distributions differ in the number of attractors and, hence, in the number of irreducible domains. With ELI-D each O-H-bond is characterized by a single irreducible domain around the corresponding hydrogen atom. In contrast, $C_{0.6}$ displays two separate domains for each O–H-bond (confront also later the discussion of Fig. 5). One of the $C_{0.6}$ attractors between the oxygen and hydrogen is due to the bond critical point of the electron density. The second $C_{0.6}$ attractor closer to the oxygen core is formed by the valence shell of oxygen (the $C_{0.6}$ shell maxima are shifted towards the nucleus, cf. Fig. 2 for the Ne atom). Thus, in the O–H-bonding region the topology of both functionals differs significantly. However, the core and lone-pair regions are similar for both distributions, with one attractor for the oxygen core and two separate attractors for the lone-pairs. The electron populations in the basins of ELI-D and $C_{0.6}$ for the water molecule, listed in Table 1, are roughly the same (sum of two basins in case of the $C_{0.6}$). Observe, that in a broad spherical region around the oxygen the values of ELI-D and $C_{0.6}$ are very similar, cf. the green belt (differences close to zero) in the bottom left diagram in Fig. 3 mapping the difference between ELI-D and $C_{0.6}$.

The upper and middle diagrams of the middle column in Fig. 3 display the 2.1-localization domains of ELI-D for the nitrogen molecule and the 1.3-localization domains of $C_{0.6}$, respectively. Both functionals exhibit the same number of attractors, but, except for the core basins, with very different electron populations in the respective basins, cf. Table 1. The basin corresponding to the triple bond contains 3.9 electrons in case of ELI-D, whereas 5.7 electrons are found for $C_{0.6}$. The electron population for the lone-pair basin is 3.0 and 2.2 for ELI-D and $C_{0.6}$, respectively. Interestingly, the population of the lone-pair basin given by $C_{0.6}$ is closer to the 'expected' 2 electrons (and correspondingly the population of the bond basin closer to 6 electrons expected for a triple bond). The differences between the two functionals, shown in the bottom middle diagram, highlight the green colored region around the N_2 molecule (except close to the nuclei) where ELI-D and $C_{0.6}$ attain similar magnitudes. Only in a narrow corridor around the bond midpoint the $C_{0.6}$ shows much higher values than ELI-D due to the low density gradient close to the bond critical point.

The 2.42-localization domains of ELI-D for the ethene molecule are presented in the upper right diagram in Fig. 3, the 1.2-localization domains of $C_{0.6}$ are shown in the middle diagram of the right column. While in the core regions both functionals show the same topology, differences appear in the C–C bonding region. ELI-D displays two separate attractors for the C–C bond, one above and the second below the molecular plane. The corresponding basins contain 1.7 electrons each, cf. Table 1. In case of $C_{0.6}$ this region exhibits a single attractor whose basin is populated by 3.5 electrons (which is close to twice the 1.7 electrons, the total population of the ELI-D C–C

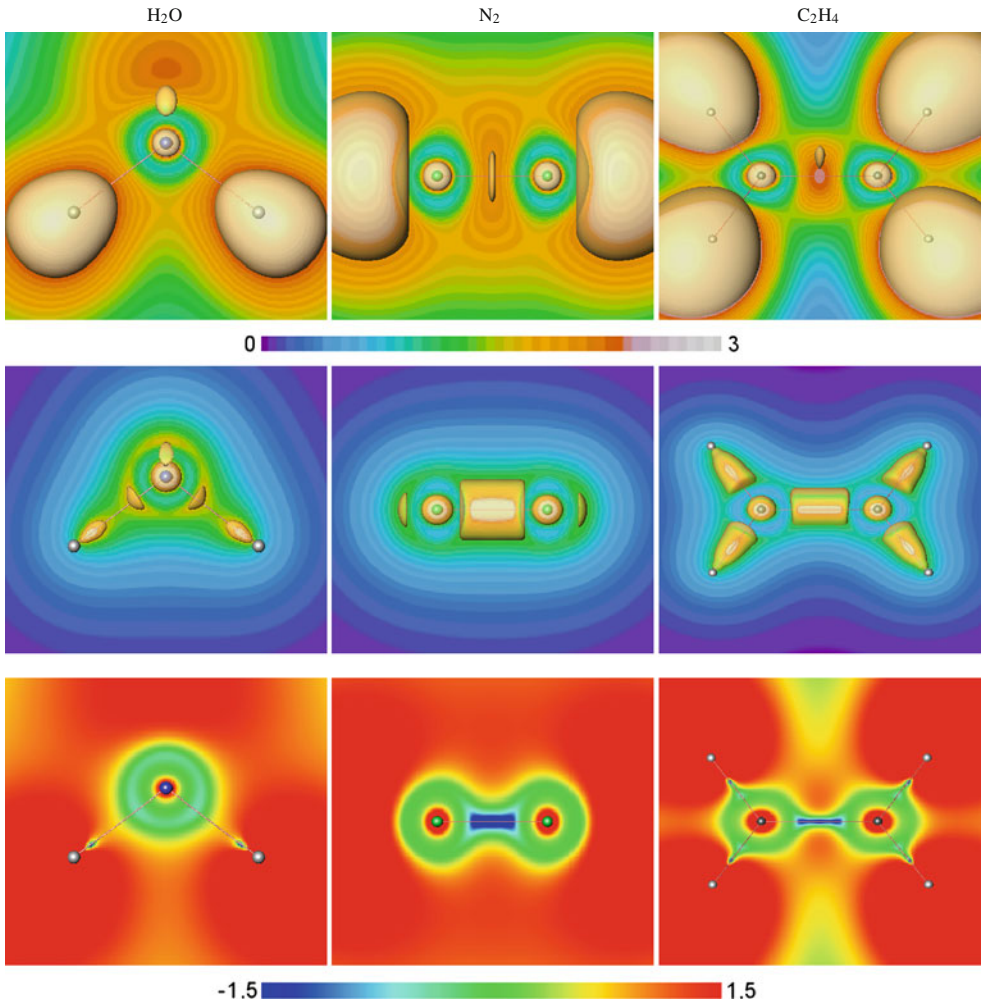

Fig. 3 $C_{0.6}$ and ELI-D for some molecules. *Left column* H_2O, *mid column* N_2, *right column* C_2H_4. *First row* triplet ELI-D from total density and localization domains for the isovalues $\Upsilon_{D^{(t)}} = 2.33(H_2O), \Upsilon_{D^{(t)}} = 2.1(N_2), \Upsilon_{D^{(t)}} = 2.42(C_2H_4)$. *Second row* $C_{0.6}$ from total density and localization domains for the isovalues, $C_{0.6} = 1.62$ (H_2O), $C_{0.6} = 1.3$ (N_2), $C_{0.6} = 1.2$ (C_2H_4). *Third row* the difference $\Upsilon_{D^{(t)}} - C_{0.6}$

Table 1 Electron population in basins of $C_{0.6}$ and $\Upsilon_{D^{(t)}}$

	H_2O		N_2		C_2H_4	
	$\Upsilon_{D(t)}$	$C_{0.6}$	$\Upsilon_{D(t)}$	$C_{0.6}$	$\Upsilon_{D(t)}$	$C_{0.6}$
Core	2.1	2.0	2.1	2.0	2.1	2.0
LP	2.2	1.8	3.0	2.2		
Bond	1.7	1.4 O	3.9	5.7	2 × 1.7	3.5 CC
		0.8 H			2.1	2.1 CH

bonding region). In the C–H bonding region both functionals display a single attractor with the corresponding basins enclosing 2.1 electrons (there is a spurious attractor for $C_{0.6}$ in the proximity of each hydrogen atom, due to the utilization of Gaussian basis set [28]). All the $C_{0.6}$ bonding attractors arise from zero electron density gradient at the bond critical points. This is also the reason for the large difference between the $C_{0.6}$ and ELI-D values around the bond midpoint, cf. the difference plot shown in the bottom right diagram. Like for the previous examples the difference of $C_{0.6}$ and ELI-D values is very low in a belt-like region around the carbon atoms.

For all examined molecules the following general trend can be observed. The localization domains of ELI-D are more wide spread (voluminous) around the molecular skeleton, whereas the localization domains of $C_{0.6}$ are relatively narrow. In regions close to the respective nuclei the $C_{0.6}$ values are lower than the ELI-D ones, cf. Fig. 2 and the three difference diagrams for the molecules in Fig. 3. The $C_{0.6}$ attractors representing the lone-pairs as well as the valence shell maxima are shifted towards the corresponding nuclei when compared with the ELI-D attractors.

As $C_{0.6}$ was optimized to resemble the ELI-D topology for atoms as close as possible, it appears quite natural that

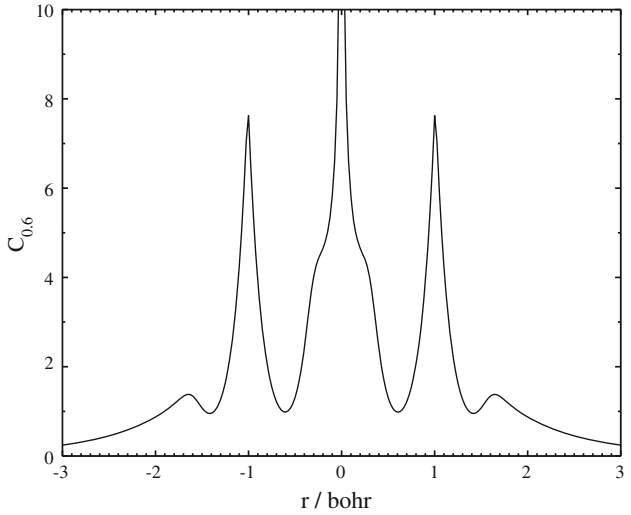

Fig. 4 $C_{0.6}$ for N_2 along the internuclear axis

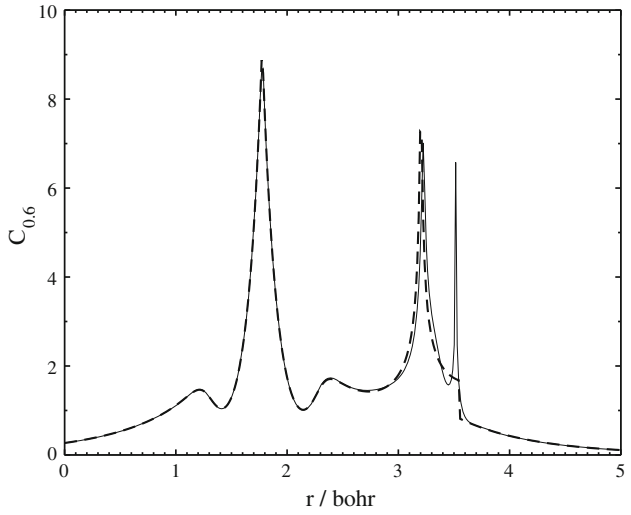

Fig. 5 $C_{0.6}$ for H_2O along the O-H bond line. *Solid line* $C_{0.6}$ for Gauss-type orbitals wavefunction (Gaussian09 HF/cc-pVQZ level), *dashed line* $C_{0.6}$ for Slater-type orbitals wavefunction (ADF HF/QZ4P level)

the inner atomic shell regions show similar structure. Remarkably, the lone-pair regions reveal similar topology of the ELI-D and $C_{0.6}$ distributions as well. In contrast, the bond regions exhibit some differences. ELI-D indicates the majority of bonds by a single attractor, whereas $C_{0.6}$ shows singly, doubly and triply indicated bonding regions, respectively. The bonding region of a diatomic molecule will always be at least singly indicated in $C_{0.6}$ due to the presence of the bond critical point in the electron density.

An example for a singly indicated bond is the nitrogen molecule. Figure 4 shows $C_{0.6}$ along the internuclear axis (bond distance 2 bohr). The core regions are marked by a peak of high $C_{0.6}$ values around the atomic positions, the lone-pair attractors are located roughly at 1.7 bohr from the bond midpoint, that is, about 0.7 bohr from the nearest nucleus. In the bonding region between the two nitrogen atoms only one separate attractor is visible. The bond peak is sharp around the critical point and broadens after a shoulder (located about 0.7 bohr from the nearest nucleus). Observe that the shoulders are at roughly same distance from the nuclei as the lone-pair attractors. It seems that the shoulders are atomic shells superimposed by the $C_{0.6}$ bond peak due to the bond critical point. The singly indicated bonding region is found for non-polar bonds.

In case of a polar bond the bond critical point is usually shifted towards the electropositive atom. This is illustrated in Fig. 5 showing $C_{0.6}$ along the O–H bond line for the water molecule. The oxygen nucleus is located at $r = 1.8$ bohr with a peak of $C_{0.6}$ indicating the oxygen core region. The two smaller peaks left and right from the core region mark the valence shell of the oxygen. The hydrogen atom is located at $r = 3.5$ bohr. The $C_{0.6}$ from the Gaussian09 calculation (solid line) exhibits a discontinuity slightly before the hydrogen position, stemming from a non-nuclear density maximum due to the rater poor performance of Gaussian functions at the atomic nuclei [28]. For the wavefunction from the ADF [29] calculation, using Slater-type functions, this discontinuity does not appear, cf. the dashed line in Fig. 5. The bonding attractor, resulting from the O–H bond critical point, is located at $r = 3.2$ bohr, close to the hydrogen atom. The $C_{0.6}$ bonding attractor does not spread widely over the bonding region, allowing the valence shell attractor of the oxygen atom to remain visible (at the position $r = 2.4$ bohr). Thus, polar-bond regions are expected to be doubly indicated.

It may also happen that the region between two atoms is described by triple indication. This case is illustrated in Fig. 6 showing $C_{0.6}$ along the internuclear line for the neon dimer (3.78 bohr was used for the interatomic distance). The peaks around the nuclear positions indicate the core regions. To the left and right of the core peaks the valence shells are visible. The $C_{0.6}$ attractor caused by the bond critical point of the electron density is located at the midpoint between the atoms. As the corresponding peak is extremely narrow, it does not disturb the forming of the valence shell attractors. The triply indicated interatomic region of the neon dimer is an example of a non-bonded situation.

The volume function $\tilde{V}_{I_p}$ for the inhomogeneity measure parameter $p = 0.6$ is not able to mimic sufficiently good the pair-volume function of ELI-D for molecules over the whole space. Polar bonds reveal significant differences between the inhomogeneity-restricted volume function and the pair-volume function. Whenever the bond critical point is shifted strongly towards one of the bonding participants, an attractor will emerge for the valence shell of the more

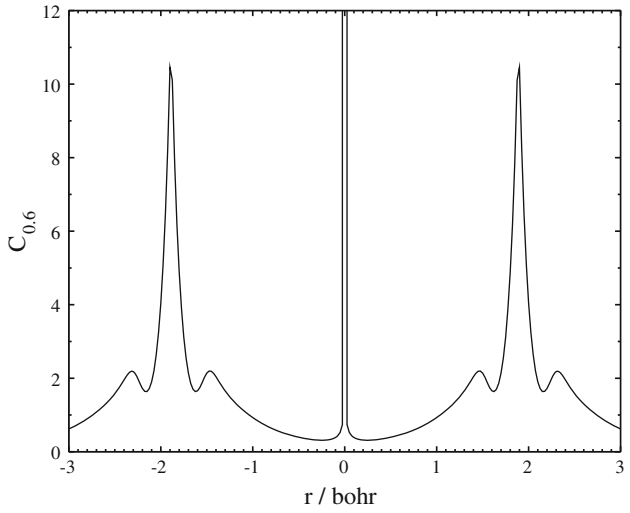

Fig. 6 $C_{0.6}$ for Ne_2 along the internuclear axis

electronegative atom. Thus, $C_{0.6}$ will display two separate attractors for polar bonds, whereas ELI-D usually shows just a single attractor. In non-polar bonds only a single attractor for $C_{0.6}$ is expected in the bond region, similarly to ELI-D for single bond (for double bond ELI-D may exhibit two attractors). In lone-pair regions the number of attractors usually coincides between $C_{0.6}$ and ELI-D. In general, the attractors of $C_{0.6}$ are shifted towards the corresponding nucleus, cf. Fig. 2.

4 Conclusions

$C_{0.6}$ is a functional based on the sampling of electron populations in very small regions (micro-cells) of fixed extent of electron density inhomogeneity. The inhomogeneity measure used is given by the distance of function values to the average within the chosen region. The distance measure depends on a parameter that can be determined by least-square fit procedure in such way that $C_{0.6}$ mimics the ELI-D topology for atoms. The optimal value (in the above sense) of the inhomogeneity parameter is $p = 0.6$. The optimal parameter value is more or less independent of the atomic species, which allows for the transferability to molecules. $C_{0.6}$ shows for molecules the inner atomic shell structure comparable to that of ELI-D. This applies also to the lone-pair regions. $C_{0.6}$ is not able to mimic ELI-D in the bonding region where both distributions may deviate significantly. In contrast to ELI-D the functional $C_{0.6}$ is applicable to experimental electron densities and thus analyses of the bonding situation using the $C_{0.6}$ signatures can be made independent of the underlying theoretical calculations.

References

1. Bader FWR (1990) Atoms in molecules—a quantum theory. Clarendon press, Oxford
2. Blanco MA, Pendas AM, Francisco E (2005) J Chem Theory Comput 1:1096–1109
3. Francisco E, Pendas AM, Blanco MA (2006) J Chem Theory Comput 2:90–102
4. Kohout M, Savin A, Preuss H (1991) J Chem Phys 95:1928–1942
5. Bohorquez HJ, Boyd RJ (2010) Theor Chem Acc 127:393–400
6. Bader RFW, Gatti C (1997) Chem Phys Lett 287:233–238
7. Gatti C, Lasi D (2007) Faraday Discuss 135:55–78
8. Hunter G (1986) Int J Quantum Chem 24:197–204
9. Sagar RP, Ku ACT, Smith VH Jr., Simas AM (1988) Can J Chem 66:1005–1012
10. Kohout M (2001) Int J Quantum Chem 83:324–331
11. Fradera X, Austen MA, Bader RFW (1999) J Phys Chem 103:304–314
12. Becke AD, Edgecombe KE (1990) J Chem Phys 92:5397–5403
13. Silvi B (2003) J Phys Chem 107:30813,085
14. Kohout M (2002) Int J Quantum Chem 97:651–658
15. Kohout M, Pernal K, Wagner FR, Grin Y (2004) Theor Chem Acc 112:453–459
16. Kohout M, Pernal K, Wagner FR, Grin Y (2005) Theor Chem Acc 113:287–293
17. Kohout M, Wagner FR, Grin Y (2008) Theor Chem Acc 119:413–420
18. Pendas AM, Kohout M, Blanco MA, Francisco E (2012) Beyond standard charge density topological analyses. In: Gatti C, Macchi P (eds) Modern charge density analyses. Springer, London
19. Wagner K, Kohout M (2011) Theor Chem Acc 128:39–46
20. Kohout M (2007) Faraday Discuss 135:43–54
21. Clementi E, Roetti C (1974) At Data Nucl Data Tables
22. Kohout M (2010) DGrid, version 4.6. Radebeul
23. Perdew JP, Chevary JA, Vosko SH, Jackson KA, Pederson MR, Singh DJ, Fiolhais C (1992) Phys Rev B 46:6671–6687
24. Perdew JP, Burke K, Ernzerhof M (1996) Phys Rev Lett 77:3865–3868
25. Perdew JP, Ernzerhof M, Zupan A, Burke K (1998) J Chem Phys 108:1522–1531
26. Haas P, Tran F, Blaha P, Schwarz K, Laskowski R (1997) Phys Rev B 80. doi:10.1103/PhysRevB.80.195109
27. Frisch MJ, Trucks GW, Schlegel HB, Scuseria GE, Robb MA, Cheeseman JR, Montgomery JA Jr, Vreven T, Kudin KN, Burant JC, Millam JM, Iyengar SS, Tomasi J, Barone V, Mennucci B, Cossi M, Scalmani G, Rega N, Petersson GA, Nakatsuji H, Hada M, Ehara M, Toyota K, Fukuda R, Hasegawa J, Ishida M, Nakajima T, Honda Y, Kitao O, Nakai H, Klene M, Li X, Knox JE, Hratchian HP, Cross JB, Bakken V, Adamo C, Jaramillo J, Gomperts R, Stratmann RE, Yazyev O, Austin AJ, Cammi R, Pomelli C, Ochterski JW, Ayala PY, Morokuma K, Voth GA, Salvador P, Dannenberg JJ, Zakrzewski VG, Dapprich S, Daniels AD, Strain MC, Farkas O, Malick DK, Rabuck AD, Raghavachari K, Foresman JB, Ortiz JV, Cui Q, Baboul AG, Clifford S, Cioslowski J, Stefanov BB, Liu G, Liashenko A, Piskorz P, Komaromi I, Martin RL, Fox DJ, Keith T, Al-Laham MA, Peng CY, Nanayakkara A, Challacombe M, Gill PMW, Johnson B, Chen W, Wong MW, Gonzalez C, Pople JA (2009) Gaussian 09, revision A.02. Gaussian, Inc., Wallingford
28. Reinhardt P, Hoggan PE (1976) Int J Quantum Chem 42:3191–3198
29. ADF200801 (2008) SCM, theoretical chemistry. Vrije Universiteit, Amsterdam. http://www.scm.com